

RESEARCH

Open Access



Electrical and thermal performance analysis of hybrid photovoltaic/thermal water collector using meta-heuristic optimization

Heba S. Aggour^{1*}, Doaa M. Atia¹, Hanaa M. Farghally¹, M. Soliman² and M. Omar²

*Correspondence:
hebasamir@eri.sci.eg

¹ Photovoltaic Cells Department,
Electronics Research Institute,
Cairo, Egypt

² Faculty of Engineering Shoubra,
Benha University, Cairo, Egypt

Abstract

The photovoltaic/thermal (PV/T) flat-panel technology has numerous advantages over PV modules and separately mounted solar thermal collectors regarding overall effectiveness and space-saving. Hybrid PV/T solar collectors' thermal and electrical performance is influenced by design parameters like mass flow rate, tube diameter, tube spacing, packing factor, and absorber conductivity. This paper focused on using several meta-heuristic optimization techniques, incorporating the following: multiverse algorithm, dragonfly algorithm, sine-cosine algorithm, moth-flame algorithm, whale algorithm, particle swarm algorithm, ant-lion algorithm, grey wolf algorithm, and particle swarm optimization algorithm in PV/T collector optimal design according to maximum total efficiency obtained. The outcomes of the various algorithms revealed that the maximum electrical efficiency of the PV/T collector ranged from 13.85 to 14.28%, while the maximum thermal efficiencies ranged from 41.41 to 52.08% under standard test conditions (1000 W/m² and 25 °C). The optimized values for the design parameters of the PV/T collector were as follows: the absorber conductivity was determined to be 356.6 W/m K, the packing factor was optimized to 0.7, the mass flow rate was set at 0.019 kg/s, the tube width was determined to be 0.035 m, and the tube spacing was optimized to 0.0524 m. The results indicated that the grey wolf optimizer (GWO) algorithm proved to be highly effective in optimizing the design parameters of PV/T collectors. Furthermore, the study examined the relationship between the temperature of PV modules and PV/T collectors by considering variations in mass flow rate, packing factor, and tube width at different solar radiation levels. The results confirmed that the PV/T collector temperature exhibited improvements compared to the PV module temperature. As a result, this led to higher electrical efficiency and an overall increase in the total efficiency of the PV/T collector.

Keywords: PV/T, Meta-heuristic optimization, Renewable energy, GWO, ALO, MVO, MFO, SCA, WOA, Efficiency

Introduction

Wolf [1] first introduced PVT (photovoltaic/thermal) technology in 1976, to increase total solar efficiency and jointly produce thermal and electrical energy. Additionally, because some of the waste heat is eliminated, the working temperature of the PV cells is reduced and as a result increases their electrical efficiency. PVT modules of all types,

such as heat pipe PVT modules, air PVT modules [2], water PVT modules [3, 4], and nanofluid PVT modules [5, 6], have been developed over many years [7]. However, the intermittent nature of solar irradiance still limits the performance of the aforementioned PVT systems. Additionally, the temperature impact causes a greater output thermal energy level (and, thus, a higher module temperature) result in a lower electrical efficiency, so there is a conflict between that level and electrical efficiency [8]. There are two ways to identify each PV/T system's optimal performance point: conducting several experiments and utilizing sophisticated computer techniques. Nowadays, computer approaches direct us to quickly and correctly find the optimal solution for each complex system [9]. In an air PV/T system, Shamsavari et al.'s [10] study concentrated on a number of certain variables, such as the channel's depth, length, and width as well as the output air temperature for system optimizing, and report the finest cases, based on NSGA.

Cao et al. [11] examined the cooling of a PV system using a nanofluid in a different investigation. They looked into the effects of three key changes in the mass flow rate, solar irradiation, as well as the nanofluid characteristics. The adaptive neuro-fuzzy inference system (ANFIS) was used to optimize the system, and the estimated procedure's optimum electrical efficiency was calculated. In 2013, Karathanassis et al. [12] developed a novel optimization approach for particular usage in a micro-channel. Khaki et al. [13] employed the genetic algorithm to improve both the energy efficiency and exergy efficiency of building integrated photovoltaic/thermal (BIPV/T) systems. Vera et al. [14] put up a mathematical model and made both experimental and mathematical predictions regarding the building integrated photovoltaic/thermal (BIPV/T) system's efficiency. To determine the best selection criteria that would affect the system's mechanism and overall performance, they used the GA. Air gap, collector length, aspect ratio, mass flow rate, collector count, and storage tank capacity were the factors that were examined. The use of GA in conjunction with optimization goals was the main focus of Singh et al. study [15]. Sohani et al. [16] performed a multi-objective optimization of a building integrated photovoltaic/thermal (BIPV/T) system using phase change material (PCM) in the context of Tehran's weather conditions. The optimization process incorporated energy efficiency, ecological impact, and economic factors to achieve a balanced outcome. Therefore, 77.2 mm was determined to be the ideal PCM thickness for the test conditions. Additionally, the energy payback period of the system was determined to be 3.3 years., and its annual CO₂ emissions were 17.7% fewer than they were been in the basic case.

A PV/T arrangement was examined by Sarhaddi et al. [17]. They demonstrated a novel method for examining the design specifications of an average air PV/T system. Moreover, electrical, thermal, and environmental aspects were considered in the total energy analysis of an air PV/T configuration. Their results demonstrated that the system under investigation had total energy, electrical, and thermal efficiency of around 45%, 10%, and 17.18%, respectively. In 2022, Sattar et al. [18] conducted the most recent study and created an analytical model for a solar module that was paired with airflow to provide cooling. The main parameters that were considered were mass flow rate, irradiation, temperature, and duct geometrical requirements. Additionally, the main optimization objective was to increase the electrical output power. A multi-objective multivariable optimization was used on the system to accomplish this goal [19].

This paper focused on studying the parameters design (the mass flow rate of fluid (m), tube spacing (W), tube diameter (D), absorber conductivity (K_{abs}), and packing factor (S)) effect on both electrical and thermal efficiencies of a PVT collector with different types of meta-heuristic algorithms: moth flame optimization (MFO), ant-lion optimization (ALO), dragonfly algorithm (DA), grey wolf optimization (GWO), particle swarm optimization (PSO), multiverse optimization (MVO), and genetic algorithm (GA). The algorithms for sine-cosine algorithm (SCA) and whale optimization (WOA) were selected and applied on multi-objective optimization problem to obtain the optimal solution of design parameters. The algorithms were built and validated using MATLAB software, comparing these algorithms' results to obtain the most accurate and useful result for collector designing. Finally, the effect of these parameters was studied as a feasibility study on the PVT collector performance represented in thermal and electrical efficiencies and mean plate temperature. Moreover, the influence of air temperature as well as solar radiation regarding the average plate temperature and both efficiencies of the PV/T collectors was studied.

The paper structure is divided into the following parts: Part 2 introduces the detailed mathematical modeling of PV/T collector. Part 3 explains the problem formulation and the different used algorithms. Part 4 discusses the optimization algorithms used in this study. Part 5 displays and talks about the results obtained from each algorithm and a comparison of the temperatures of the hybrid PV/T collector and PV modules in different environmental conditions. Finally, "Conclusions" Section presents the conclusions and recommendations.

Mathematical model

Here, a water PV/T system's mathematical model was created using the energy balances of its many parts. Due to the system's symmetrical geometry, differential elements with length (dx) as well as width (w) were used (Fig. 1).

The collector's useful energy output is [21]:

$$Q_u = S \cdot A_{PV/T} F_R [G(\tau\alpha)_{eff} - U_L(T_i - T_a)] + (1 - S) [A_{PV/T} F_R [G(\tau\alpha)_{eff} - U_L(T_{pm} - T_a)]] \tag{1}$$

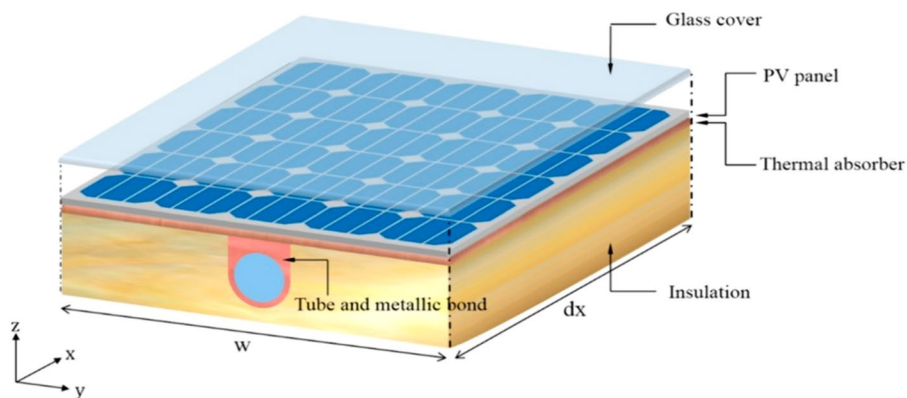


Fig. 1 PV/T system schematic view [20]

where the area of PV/T collector is $A_{PV/T}$, the PV plate average temperature is T_{pm} , the ambient temperature is represented by T_a , the heat removal factor is given by F_R , the solar irradiance is represented as G , T_i represents the water input temperature, S is the area of the PV/T module covered with the PV cell, and the total heat loss coefficient is given by U_L . The heat removal factor is determined as follows [22]:

$$F_R = \frac{mC_p}{A_{PV/T}U_L} \left[1 - \frac{\frac{Z}{U_i} - (T_o - T_a)}{\frac{Z}{U_i} - (T_i - T_a)} \right], \tag{2}$$

where Z is the solar energy absorbed, T_o is the temperature of the outlet water, T_i is temperature of the inlet water, m is the water flow rate, and C_p is the specific heat coefficient of water (constant pressure). The overall heat loss coefficient is [23]:

$$U_L = U_t + U_b + U_e, \tag{3}$$

where U_e is the edge's heat loss coefficient, the backside's heat loss coefficient is U_b , and U_t is the front side's total heat loss coefficient. The next equation can calculate the total efficiency, electrical efficiency, and thermal efficiency [22, 23]:

$$\eta_{th} = \frac{Q_u}{A_{PV/T} \cdot G}, \tag{4}$$

$$\eta_{elect} = \eta_{e,ref} [1 - B(T_{cell} - T_{a,ref})], \tag{5}$$

$$\eta_T = \eta_{th} + \frac{\eta_{elect}}{\eta_{plant}}, \tag{6}$$

where T_{cell} is the PV cells 'temperature, $T_{a,ref}$ indicates the temperature under standard conditions (298.15 K), B indicates the PV temperature coefficient (0.0045), $\eta_{e,ref}$ is the solar cell's efficiency under STC, η_T indicate the total efficiency, the thermal efficiency is η_{th} , and η_{elect} indicates the total efficiency, and η_{plant} is the average efficiency of producing electrical power and is taken as 38%.

The study was performed in the city of Cairo (30.06° N, 31.23° E). The monthly solar radiation as well as air temperature of Cairo, Egypt, is indicated in Fig. 2. Table 1 illustrates the parameters of PV/T collector [23].

Problem formulation

Several valuable studies have been conducted to optimize PV/T collectors design parameters (the fluid flow rate (m), tube space (W), absorber conductivity (K_{abs}), tube diameter (D), and packing factor (S) using various techniques. Certain studies revised the optimization algorithms to improve PV/T collector performance and efficiency. This study enhanced the PV/T collectors' effectiveness, with several optimization techniques (GA, PSO, GWO, ALO, MVO, DA, MFO, SCA, and WOA) for obtaining the desired optimal system design corresponding to the highest efficiency. Using optimization methods, the optimized operating parameters for PV/T collectors were found with high thermal and electrical efficiency as the objective. There are five factors in the desired PV/T collector, which are represented as:

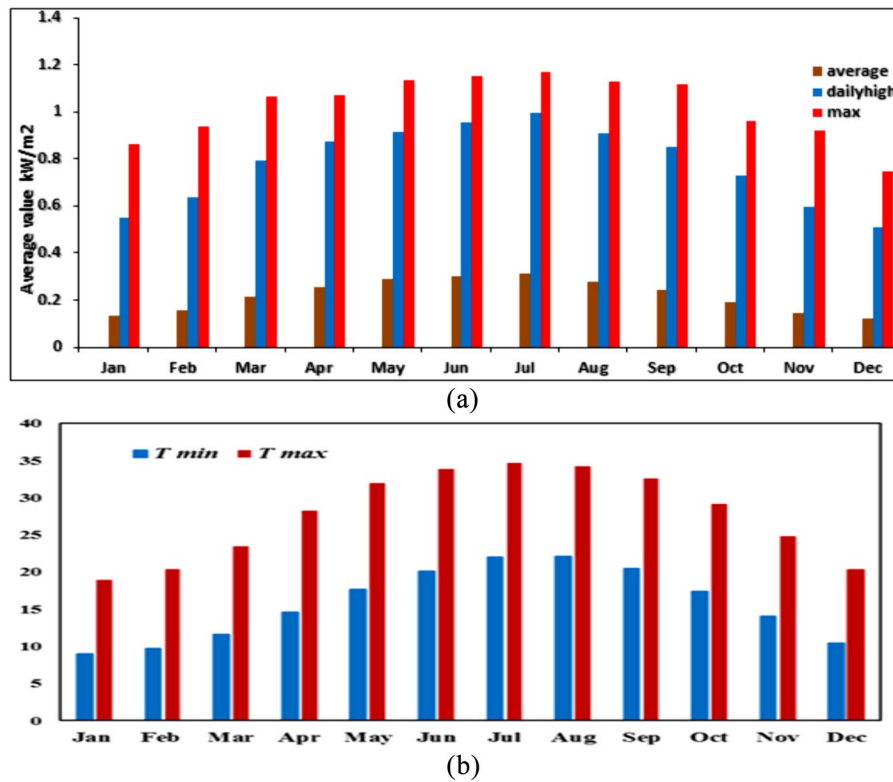


Fig. 2 Monthly environmental condition of Cairo a solar radiation b air temperature [24]

Table 1 Configuration parameters of PV/T collector

PV/T layers	Parameters	Units
PV/T collector	Area	1.6 (m ²)
	Length	1.6 (m)
	Width	1 (m)
Glazing	Thickness	0.004 (m)
	Thermal conductivity	0.9 (W/m K)
	Emissivity	0.8
	Transmissivity	0.92
	Absorptivity	0.04
	Thermal conductivity	84 (W/m K)
	Absorptivity	0.95
Absorber plate	Emissivity	0.88
	Packing factor	1
	Temperature coefficient	0.45 (%/K)
	Thermal conductivity	360 (W/m K)
	Thickness	0.07 (m)
Tube	Tube diameter	0.01 (m)
	No. of tubes	12
	Tube spacing	0.0795 (m)
	Mass flow rate	0.02 (kg/s)
Insulation	Thickness	0.07 (m)
	Thermal conductivity	0.033 (W/m. K)

$$x_i^{\min} \leq x_i \leq x_i^{\max}; i = 1, 2, 3, 4, 5 \tag{7}$$

where $x = (m, D, W, K_{abs}, S)$.

The optimal values of x_i were determined by maximizing the thermal and electrical efficiencies of the PV/T collector in which the objective function is given by:

$$f(x) = \max \left\{ \begin{array}{l} \eta_{e,ref} [1 - B(T_{cell} - T_{a,ref})] \\ \frac{Q_u}{A_{PV/T} G} \\ \eta_{th} + \frac{\eta_{elect}}{\eta_{plant}} \end{array} \right. \tag{8}$$

The objective functions for maximizing the provided efficiencies are determined as follows:

$$f(x)_{\min} = \min \left(\frac{1}{f(x)} \right) \tag{9}$$

As the provided objective function is minimized, the efficiencies will be maximized.

Optimization algorithms

Genetic algorithm

A GA is a popular and extensively utilized tuning technique based on natural selection and genetics. Furthermore, it is often employed as a baseline for assessing sophisticated algorithms. The Global Optimization Toolbox in MATLAB was used in this study for GA optimization. It is a versatile tool to find results rapidly and efficiently.

Particle swarm optimization

This algorithm is initiated by a swarm of particles (the initial population). Particles use precise formulas to search across the search region. Particles attend their finest-recognized places after conducting the study in the field of search. Next, the ideal position is determined, and the particles control the movement of extra particles. The exploration of the field of search is repeated until a proper result is recognized. The swarm is fine-tuned according to the equations below for each iteration [25]:

$$v_i^{t+1} = I * v_i^t + c_1 * r_1 * (p_i^t - x_i^t) + c_2 * r_2 * (g_i^t - x_i^t), \tag{10}$$

$$x_i^{t+1} = x_i^t + v_i^{t+1}, i = 1, 2, \dots, n \tag{11}$$

where I indicates the weighted inertia, positive constants are c_1 and c_2 , n indicates number of particles, plus t indicates the iterations' number, and r_1 and r_2 are two random variables that diverge within the interval 0 and 1. The particle's finest location is p_i , while its biggest particle is g_i .

Grey wolf optimization algorithm

This algorithm is stimulated by means of the headship construction and shooting performance of grey wolves (*Canis Lupus*) in their normal habitation. The headship construction in the model simulation is separated into four wolf classifications: alpha,

delta, beta, and omega. The stages of shooting are as follows: looking for a target, rotating it, and attacking it [26]. The rightest result is observed in the alpha (α) that mathematically simulated the social hierarchy of wolves in GWO. Subsequently, the results indicate that beta (β) and delta (δ) are the second and third highest scores. Omega (ω) is expected for the outstanding probable results. The GWO algorithm's optimization is guided by α and β ; these wolves are followed by means of the ω wolves [27]. The next is a short-lived description of the mathematical model. The circling routine of the grey wolves is mathematically denoted by [28]:

$$\vec{D} = \left| \vec{c} \cdot \vec{x}_p(\text{iter}) - \vec{x}(\text{iter}) \right|, \tag{12}$$

$$\vec{x}(\text{iter} + 1) = \vec{x}_p(\text{iter}) - \vec{A} \tag{13}$$

The position vectors of the prey and grey wolves are represented by \vec{x}_p and \vec{x} , respectively. The current iteration is iter. Coefficient vectors \vec{A} and \vec{B} are estimated as follows [29]:

$$\vec{A} = 2\vec{a}\vec{r}_1 - \vec{a}, \tag{14}$$

$$\vec{C} = 2\vec{r}_2, \tag{15}$$

where \vec{r}_1 , and \vec{r}_2 are the random vectors with values between 0 and 1. Through the iterations, the components of a are progressively lowered from 2 to 0. Grey wolf hunting is mathematically modeled as follows [29]:

$$\vec{D} = \left| \vec{b}_1 \vec{x}_a - \vec{x} \right|, \vec{D}_\beta = \left| \vec{b}_2 \vec{x}_\beta - \vec{x} \right|, \vec{D}_\delta = \left| \vec{c}_3 \vec{x}_\delta - \vec{x} \right|, \tag{16}$$

$$\vec{x}_1 = \vec{x}_a + \vec{A}_1(\vec{D}_a), \vec{x}_2 = \vec{x}_\beta + \vec{A}_2(\vec{D}_\beta), \vec{x}_3 = \vec{x}_\delta + \vec{A}_3(\vec{D}_\delta), \tag{17}$$

$$\vec{x}(\text{iter} + 1) = (\vec{x}_1 + \vec{x}_2 + \vec{x}_3) / 3, \tag{18}$$

Iteratively, α , β , and δ estimate the potential target location and update the distance. The best outcomes are then used to force the other agents to update their locations. Potential solutions often converge on prey if $|A| < 1$, or flee from prey if $|A| > 1$.

Ant-lion optimization algorithm

This algorithm is built on the hunting machinery of ant-lions also includes a random way of walking exploration and haphazard agent selection. The six basic processes of the haphazard wandering of ants, catching in ant-lion pits, creating traps in ant-lions, sliding ants near ant-lions, gathering prey, and repairing traps are elitism. The elite ant-lion is selected from each iteration's greatest ant-lion. Using a stochastic movement, ants can readily detect the food location. The following equations mathematically express this phenomenon [30]:

$$y(t) = \begin{bmatrix} 0, \text{cumsum}(2r(t_1) - 1), \text{cumsum}(2r(t_2) - 1), \dots \\ \text{cumsum}(2r(t_n) - 1) \end{bmatrix}, \tag{19}$$

where $y(t)$ represents random ant walks, the variables n, t , and $r(t)$ indicate the iterations' maximum number, random walk steps, as well as the function built as follows [30]:

$$r(t) = \begin{cases} 1 & \text{rand} > 0.5 \\ 0 & \text{rand} \leq 0.5 \end{cases}, \tag{20}$$

where the symbol rand indicated a uniformly distributed random number in the range 0 and 1[31].

Multiverse optimization algorithm

Concerning the multiverse theory, there was more than just one enormous bang, but also numerous big bangs occurred, each of which birthed a novel universe. It is concluded that there are numerous other worlds besides the Earth. There is also a chance that these different universes will strike; Consequently, MVO draws inspiration for solving the optimization problem from the ideas behind worm holes, black holes, and white holes. This algorithm needs to track these optimization criteria [32].

1. The high inflation rate results in a lot of white holes.
2. Black holes are likely to exist if the rate of inflation is high.
3. If the pace of inflation in the universe is high, objects will be hurled into white holes.
4. If the rate of inflation of the universe is low, objects will be captured by black holes.
5. Objects can randomly go through wormholes to the best universe, regardless of the rate of inflation.

The following is the expression for the MVO algorithm's basic mathematical model [33]:

$$x_i^j = \begin{cases} x_k^j & r_1 < \text{NI}(U_i) \\ x_i^j & r_1 \geq \text{NI}(U_i) \end{cases}, \tag{21}$$

where $\text{NI}(U_i)$ indicates the normalized inflation rate of the i th universe, x_k^j indicates the j th object of the k th universe, a random number within 0 and 1 is r_1 , and x_i^j is the j th object of the i th universe. The equation stated x_i^j is [32]:

$$x_i^j = \begin{cases} (X_j + \text{TDR} \times (\text{ub}_j - \text{lb}_j) \times r_4 + \text{lb}_j), & r_3 < 0.5 \\ (X_j - \text{TDR} \times (\text{ub}_j - \text{lb}_j) \times r_4 + \text{lb}_j), & r_3 \geq 0.5, r_2 < \text{Wep}, \\ X_i^j & r_2 \geq \text{WEP} \end{cases}, \tag{22}$$

where TDR and WEP are coefficients, ub indicate the upper limit, lb indicate the lower bound, X_j indicate the j th parameter of the best universe discovered so far, as well as (r_2, r_3 , and r_4) are values randomly selected within 0 and 1. Adaptive factors like WEP and TDR are employed to create exploitation. WEP is used to improve exploitation near the greatest result found so far, and TDR is used to improve exploitation near the finest result found so far. The following are the WEP and TDR coefficient adaptive formulas [33]:

$$WEP = \min + l \times \left(\frac{(\max - \min)}{L} \right), \tag{23}$$

$$TDR = \left(1 - \frac{l^{\frac{1}{p}}}{L^{\frac{1}{p}}} \right), \tag{24}$$

The smallest and greatest values are characterized by min and max, in turn; l indicates the current iteration, and L is the iterations' maximum number. The exploitation factor is represented by p .

Dragonfly algorithm

This algorithm built on swarm intelligence established by Mirjalili at Griffith University in 2016. It draws inspiration from the natural dragonfly's static and dynamic behaviors [34]. Dragonflies' dynamic swarming behavior generates a variety of solutions in DA, enhancing the algorithm's exploration capabilities. The exploitation capacity of the algorithm is indicated by the static swarm [35].

The separation's mathematical model is computed as follows [34]:

$$S_i = - \sum_{j=1}^N X - X_j, \tag{25}$$

where N indicates the neighboring individuals' number, X_j indicates the j th neighboring individual position, and X indicates the current position. Alignment (A) is represented as [34]:

$$A_i = \frac{\sum_{j=1}^N V_j}{N}, \tag{26}$$

where V_j indicates the individual velocity of the j th neighbor. Cohesion (C) is computed as follows [33]:

$$C_i = \frac{\sum_{j=1}^N X_j}{N} - X \tag{27}$$

A food source's (F) attractiveness is ascertained by [34]:

$$F_i = X^+ - X \tag{28}$$

The following determines how to divert an adversary (E) externally [35]:

$$E_i = X^- + X, \tag{29}$$

in which the adversary position is denoted by X^- and the food source position by X^+ .

The dragonfly's position is updated in a search space and analysis based on its movement step vectors (ΔX) and position (X) vectors. Because DA's step vector and PSO's step vector are identical, the movement direction is indicated by DA's step vector as [35]:

$$\Delta X_{t+1} = (nS_i + aA_i + dC_i + fF_i + eE_i) + r\Delta X_t, \tag{30}$$

where the variables t, f, e, r, n, d , and A represent the number of iterations, food factor, enemy factor, weight of inertia, separation weight, cohesion weight, and alignment of the i th individual. Calculating the location vectors is done as [35]:

$$X_{t+1} = X_t + \Delta X_{t+1} \tag{31}$$

When there are no nearby alternatives, dragonflies adopt the Lévy flight walk to increase the randomness of their flight. As a result, updates the dragonfly's position by [36]:

$$X_{t+1} = X_t + \text{Levy}(d) \times X_t, \tag{32}$$

$$\text{Levy}(x) = 0.01 \times \frac{\sigma_d r_1}{|r_2|^{\frac{1}{\beta f}}}, \tag{33}$$

$$\sigma_d = \left(\frac{\Gamma(1 + \beta f) \times \sin\left(\frac{\pi \beta f}{2}\right)}{\Gamma\left(\frac{1 + \beta f}{2}\right) \times \beta f \times 2^{\left(\frac{\beta f - 1}{2}\right)}} \right)^{\frac{1}{\beta f}}, \tag{34}$$

$$\Gamma(x) = (x - 1), \tag{35}$$

where the location vectors' dimension is indicated by the letter d . With respect to $[0, 1]$, r_1 and r_2 are random values, while βf is a constant (1.5) [35].

Moth-flame optimization algorithm

The first step in MFO is the randomly generated building of moths across the solution space. Each moth's fitness value, or position, is then calculated, and the ideal position is flame-tagged. The locations of the moths are then updated by a spiral movement function for achieving the well locations tagged by a flame, then, until the termination requirements are satisfied, updating the novel finest solitary locations and repeating the earlier steps (i.e., updating the moth positions and creating new positions) [37]. The MFO mathematical model consists of two parts: flames and moths. The real search agents that traverse the search space are moths, and the best sites for moths to be found that have been found so far are fires. [38]. The following equations explain the algorithm [37]:

$$\text{No. of flame} = \text{round}\left(N - I * \frac{N - I}{T}\right), \tag{36}$$

where I denotes the current iteration, T and N denotes the maximum number of iterations and the maximum number of flames. One can determine the distance, D_i , between the j th moth (M_j) and the matching j th flame (F_j) by referring to [38]:

$$D_i = |F_j - M_j| \tag{37}$$

Sine-cosine algorithm

This algorithm [34] is motivated by sine and cosine functions. The technique searches the candidate solution space using a mathematical model to catch the optimized solution. In the search space, the particle positions are updated as [39]:

$$J_{t+1} = J_t + r_1 \cdot \sin r_2 \cdot |r_3 p - J_t| \tag{38}$$

$$J_{t+1} = J_t + r_1 \cdot \cos r_2 \cdot |r_3 p - J_t| \tag{39}$$

The updated position is J_{t+1} ; r_1 , r_2 , and r_3 are the random variables; and the desired location is Pi. Depending on if the random number is larger or smaller than 0.5, these two equations are employed accordingly. To identify the optimized solution, the particle variation in the search space is related to sine or cosine functions.

Whale optimization algorithm

A school of little fish moving close to the water surface is hunted by a humpback whale, according to Mirjalili and Lewis, who first created this algorithm in 2016. By reducing its circle, the whale creates bubbles, which can be referred to as 9-shaped routes [40]. This algorithm is split into two sections. The first step is exploration, which includes a random approach to finding prey. The spiral bubble-net attack can be used to encircle prey in the second phase, also known as the exploitation phase [41].

If $P < 5$ where P indicates a random number within 0 and 1 and if $|\vec{A}| < 1$, use the encircling prey approach to update the position [41]:

$$\vec{X}(t + 1) = \vec{X}^*(t) - (\vec{A}\vec{D}) \tag{40}$$

$$\vec{A} = (2\vec{a}\vec{r}) - (\vec{a}), \tag{41}$$

$$\vec{D} = \left| (2\vec{r}\vec{X}^*(t)) - \vec{X}(t) \right|, \tag{42}$$

where $\vec{X}(t + 1)$ represents the updated position, $\vec{X}^*(t)$ represents the best solution position, \vec{a} is a random vector between 2 and 0 depending on the maximum iteration number consuming shrinking encircling, and \vec{r} denotes a random vector in between [0, 1].

If $|\vec{A}| > 1$, update the position by exploring the phase method that [42]:

$$\vec{X}(t + 1) = \vec{X}^{rand} - (\vec{A}\vec{D}) \tag{43}$$

$$\vec{D} = \left| 2\vec{r}\vec{X}^{rand} - \vec{X}^*(t) \right| \tag{44}$$

where \vec{X}^{rand} is a random position vector.

If $P > 1$, position is updated by updating the spiral as [43]:

$$\vec{X}(t + 1) = \left(\vec{D}e^{bi \cos 2\pi l} \right) \vec{X}(t), \tag{45}$$

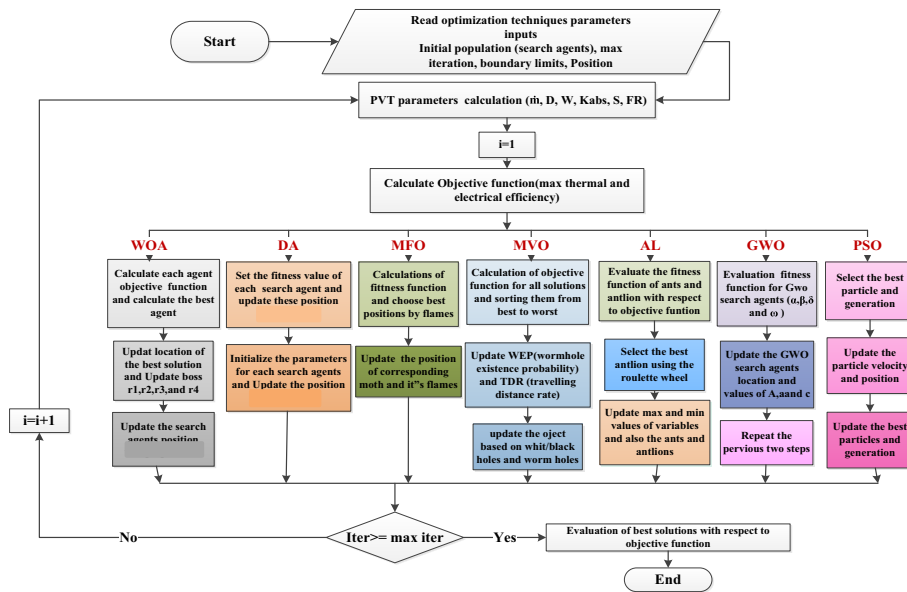


Fig. 3 Flow chart of proposed optimization algorithms for PV/T collector

Table 2 The range of variation and input parameters for optimization approaches

Parameters	Variation range	
	Lower bound	Upper bound
m (Kg/s)	0.001	0.1
D (m)	0.001	0.1
W (m)	0.001	0.1
K_{abs} (W/m K)	100	500
S	0.7	1
Iteration No	100	
Population No	500	
Agents No	50	

where L indicates a random value between -1 and 1 , and b characterizes the logarithmic spiral shape [41].

$$\vec{D} = (\vec{X}^*(t) - (\vec{X}(t))) \tag{46}$$

The flowchart introduces the steps of the previous algorithms and the explanation is shown in Fig. 3; the first step determines the optimization technique inputs parameters such as initial population, max iteration, boundary limit, and position after the calculation of PV/T parameters (m, D, W, S, K_{abs}) and calculate the objective function thermal and electrical efficiencies, set the fitness value for each search agent and update these positions, at max. Iteration evaluates the solutions with respect to objective function. Table 2 illustrates the range of variation and input parameters for optimization algorithms and approaches.

Results and discussion

This paper optimized five dissimilar PV/T collector parameters which affect the PV/T collectors overall performance. The additional design parameters remained unchanged, while these five parameters were optimized. Several design criteria should be chosen to turn a PV module with a certain size and electrical qualities into a PV/T collector. A comparison of the optimization algorithms' outcomes is displayed in Table 3. The primary design parameters are the fluid flow rate of fluid (m), tube spacing (W), tube diameter (D), absorber conductivity (K_{abs}), and packing factor (S). A comparison was made of the thermal, electrical, and overall efficiency. It was observed that ALO, SCA, and WOA produced the best fluid flow rates that are 0.025 kg/s, 0.028 kg/s, and 0.024kg/s, respectively, compared with those of other algorithms, but the SCA had the least thermal and electrical efficiencies that are 46.89%, and 14.28% respectively, compared with those of ALO and WOA, ALO efficiencies are 52.08% and 14.28, WOA efficiencies are 51.75% and 14.26%. The best tube diameter results were obtained from the PSO and MFO algorithms that is 0.01m; however, the MFO algorithm produced the best thermal and electrical efficiency that are 52.04% and 14.28%, respectively. Moreover, ALO and WOA produced optimal tube spacings, which is 0.0869 m for ALO and 0.09 m for WOA, with convergent electrical and thermal efficiencies. The absorber conductivity of copper material was obtained from the SCA optimization with thermal efficiency of 46.89% and electrical efficiency of 14.13%, and the MVO algorithm produced aluminum as an absorber material with thermal efficiency is 51.99% and electrical efficiency is 14.28%. The MVO algorithm had the highest thermal and electrical efficiencies are 51.99% and 14.28%, respectively, but copper is more cost-effective than aluminum. The optimal packing factor was obtained from the optimization results achieved using the GA, PSO, and SCA, which are 0.989, 1, and 0.9387, respectively. As shown, the GA algorithm had the worst thermal and electrical efficiencies are 41.41% and 13.85%. After the optimization process, the DA algorithm offered a better thermal efficiency is 41.89%, compared with that of the GA algorithm; however, when DA's performance was contrasted with other algorithms, it was worse. The PSO algorithm had a better tube diameter and optimized packing factor; however, it had low thermal and electrical efficiencies that are 42.44% and 13.93%, respectively. Although the SCA had good results for the flow rate, absorber conductivity, and packing factor, in addition, its thermal and electrical

Table 3 PV/T design parameters based on different optimization techniques

Algorithm	GA	PSO	GWO	ALO	MVO	DA	MFO	SCA	WOA
m (Kg/s)	0.095	0.1	0.019	0.025	0.09	0.05	0.036	0.028	0.024
D (m)	0.058	0.01	0.035	0.038	0.073	0.083	0.01	0.0032	0.0258
W (m)	0.026	0.01	0.0524	0.0896	0.0593	0.054	0.031	0.0423	0.0999
K_{abs} (W/m k)	326	221	356.6	200.83	152.8	287.9	199.5	383.9	334.5
S	0.989	1	0.7	0.7	0.7016	0.7601	0.7	0.9387	0.7
η_{th} %	41.41	42.44	52.08	52.08	51.99	41.89	52.04	46.89	51.75
η_{elec} %	13.85	13.93	14.28	14.28	14.28	13.67	14.28	14.13	14.26
η_T %	77.85	79.09	89.65	89.65	89.56	77.86	89.61	84.07	89.27

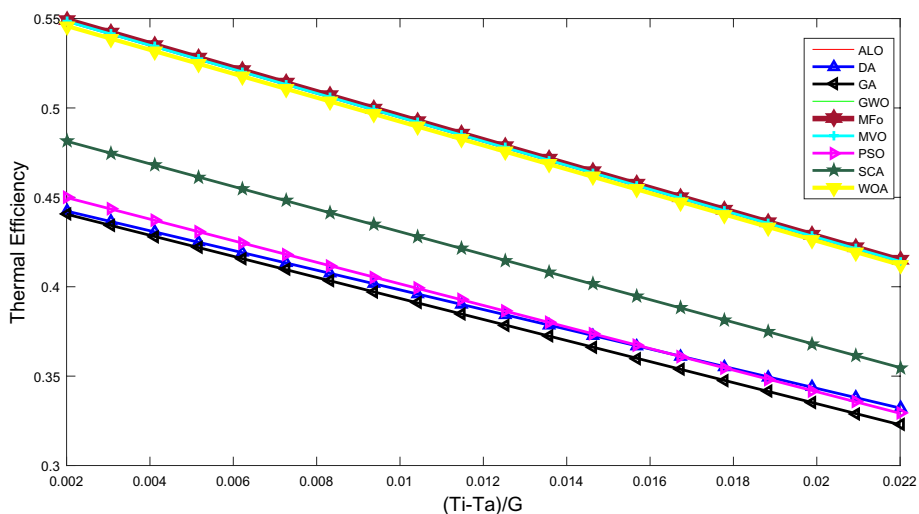


Fig. 4 Variation in thermal efficiency of PV/T for all algorithms

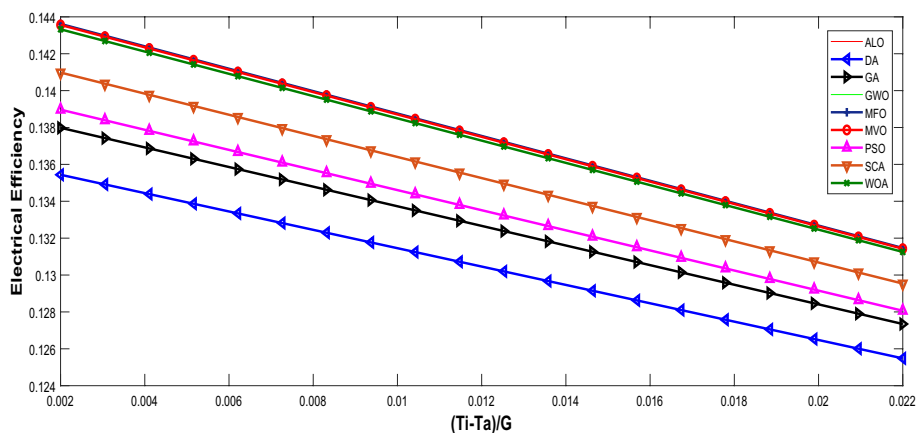


Fig. 5 Variation in electrical efficiency of PV/T for all algorithms

efficiency were poor when contrasted with other methods. With respect to the table, the electrical and thermal efficiencies of the WOA and MVO were approximately close, but the WOA values were better than the MVO values; however, they both did not have the optimal design for the PV/T collector. Finally, the MFO, ALO, and GWO algorithms had the optimized values for the both efficiencies, and the GWO algorithm had the optimal values for the design parameters. Thus, the optimized PV/T design was obtained from the GWO algorithm.

After applying the resulting optimized parameters in the simulation for each optimization algorithm, the figures of electrical and thermal efficiencies with reduced temperature were introduced. Figures 4, 5 and 6 show the comparison of each algorithm’s thermal, electrical, and total efficiencies. GWO and ALO algorithms show the same and highest electrical and thermal efficiencies, but the GWO algorithm parameters were more effective than that of the ALO algorithm.

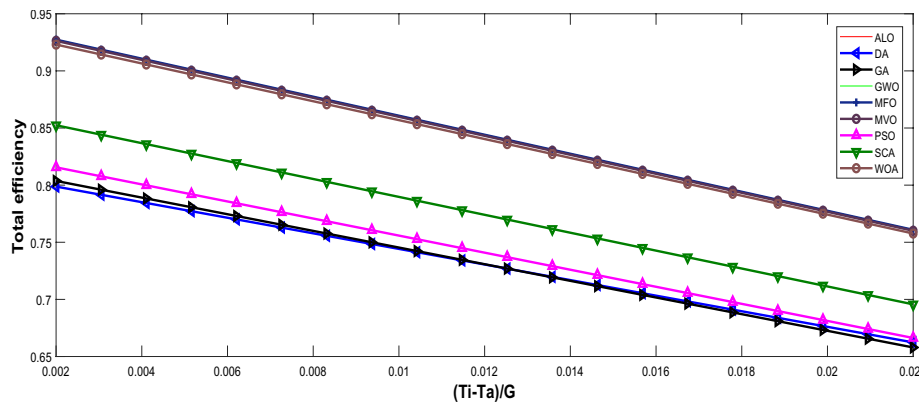


Fig. 6 Total PV/T efficiency variation for all algorithms

Table 4 The electrical, thermal, and PV/T temperature with mass flow variation

m (Kg/s)	Rad = 500 W/m ² $T_{pv} = 40\text{ }^\circ\text{C}$			Rad = 800 W/m ² $T_{pv} = 49\text{ }^\circ\text{C}$			Rad = 1000 W/m ² $T_{pv} = 55\text{ }^\circ\text{C}$		
	η_{th} (%)	η_{elec} (%)	T_{pm}	η_{th} (%)	η_{elec} (%)	T_{pm}	η_{th} (%)	η_{elec} (%)	T_{pm}
0.01	35.35	14.01	39.62	37.35	13.56	46.26	38.01	13.27	50.68
0.02	37.36	14.10	38.27	39.47	13.72	43.99	40.17	13.46	47.79
0.03	38.06	14.14	37.80	40.21	13.77	43.19	40.92	13.53	46.78
0.04	38.42	14.15	37.56	40.59	13.80	42.79	41.31	13.56	46.27
0.05	38.64	14.16	37.42	40.82	13.82	42.54	41.54	13.59	45.96
0.06	38.78	14.17	37.32	40.97	13.83	42.08	41.70	13.60	45.75

As shown from the results, the three algorithms GA with thermal efficiency of 41.41% and electrical efficiency 13.85%, PSO with thermal efficiency of 42.44% and electrical efficiency 13.39%, and DA with thermal efficiency of 41.89% and electrical efficiency 13.67%, introduce the minimum thermal and electrical efficiency values. The DA and GA had the worst values for thermal and electrical efficiencies, although GA and PSO had the maximum and most effective packing factors that are 0.095 and 1, respectively.

The thermal efficiency of the MFO and MVO algorithms was good but lower than that of the GWO and ALO algorithms. In addition, the electrical efficiency of the MFO and MVO algorithms was high but not suitable, compared with that of the GWO algorithm. The WOA algorithm efficiencies curves were high and exhibited good results, but the optimized parameters are not the most valuable values. The SCA algorithm efficiencies values were not the worst or maximum values, compared with those of other algorithms, although it had a good packing factor. Unfortunately, the other SCA parameters were not the best values. Finally, the GWO algorithm recorded the best-optimized parameters with the optimized electrical and thermal efficiencies and good design parameters.

Tables 4, 5 and 6 introduce the effectiveness of the flow rate, packing factor, and tube spacing based on the thermal and electrical efficiencies of the PV/T collector concerning the change in solar radiation. The figures show a comparison of the IV curves of a stand-alone PV and the IV curves of a PV/T collector concerning this effect at air temperature (25 °C). As shown in Table 4, it was observed that with an increase in radiation, the flow

Table 5 The electrical, thermal, and PV/T temperature with packing factor variation

S	Rad = 500 W/m ² T _{pv} = 40 °C			Rad = 800 W/m ² T _{pv} = 49 °C			Rad = 1000 W/m ² T _{pv} = 55 °C		
	η _{th} (%)	η _{elec} (%)	T _{pm}	η _{th} (%)	η _{elec} (%)	T _{pm}	η _{th} (%)	η _{elec} (%)	T _{pm}
0.2	47.93	13.94	40.73	50.03	13.45	47.92	50.73	13.13	52.71
0.4	45.27	13.98	40.13	47.36	13.52	46.96	48.06	13.21	51.52
0.6	42.60	14.02	39.53	44.70	13.58	46.01	45.40	13.29	50.32
0.8	39.93	14.06	38.94	42.03	13.65	45.05	42.73	13.37	49.13
1	37.26	14.10	38.34	39.36	13.71	44.10	40.06	13.45	47.94

Table 6 The thermal, electrical, and PV/T temperature with tube width variation

W (m)	Rad = 500 W/m ² T _{pv} = 40 °C			Rad = 800 W/m ² T _{pv} = 49 °C			Rad = 1000 W/m ² T _{pv} = 55 °C		
	η _{th} (%)	η _{elec} (%)	T _{pm}	η _{th} (%)	η _{elec} (%)	T _{pm}	η _{th} (%)	η _{elec} (%)	T _{pm}
0.01	43.7	14.15	37.6	45.93	13.80	42.78	46.67	13.57	46.24
0.02	43.10	14.12	38	45.30	13.75	43.46	46.03	13.51	47.10
0.03	42.52	14.10	38.4	44.68	13.71	44.12	45.40	13.45	47.93
0.04	41.95	14.07	38.78	44.08	13.67	44.76	44.79	13.40	48.73
0.05	41.39	14.04	39.15	43.50	13.62	45.38	44.20	13.34	49.54
0.06	40.86	14.02	39.51	42.93	13.58	45.99	43.63	13.29	50.31

rate also increased, resulting in higher thermal and electrical efficiencies. Table 5 shows that an increase in packing factor to radiation resulted in thermal efficiency decrease and an increase in electrical efficiency, but the tube spacing has a different effect on the flow rate and packing factor as it decreased the electrical and thermal efficiencies because of an increase in plate temperature. Table 6 shows the thermal, electrical, and PV/T temperature with tube width variation.

Figures 7 and 8 show similar currents in the stand-alone PV module and PV/T collector but a small change and an increase in voltage increased the flow rate and packing factor. For the stand-alone PV module, the packing factor and mass flow were less than those in the PV/T collector. Figure 9 denotes the matching currents in the stand-alone PV and PV/T collectors. However, an increase in voltage occurred in the PV/T collector and caused a decrease in tube spacing.

Table 7 shows the comparison of the present results of the optimization design with the reported results. For the GWO algorithm result (the best results obtained), Fuentes et al. [28] achieved approximately the same electrical and thermal efficiencies as those of the present efficiencies, but the total efficiency of the GWO algorithm was more effective. Compared with the other papers, the thermal, electrical, and total efficiencies of the GWO algorithm were better and more effective. Thus, the GWO algorithm had an excellent result, compared with those of the previous studies. By comparing our previous work [22] with the present study; the new algorithms overcome the lakes and disadvantages such as; inefficiency in large-scale continuous situations; great accuracy requires proper parameter adjustment, random selection of seeds and positions, and increase

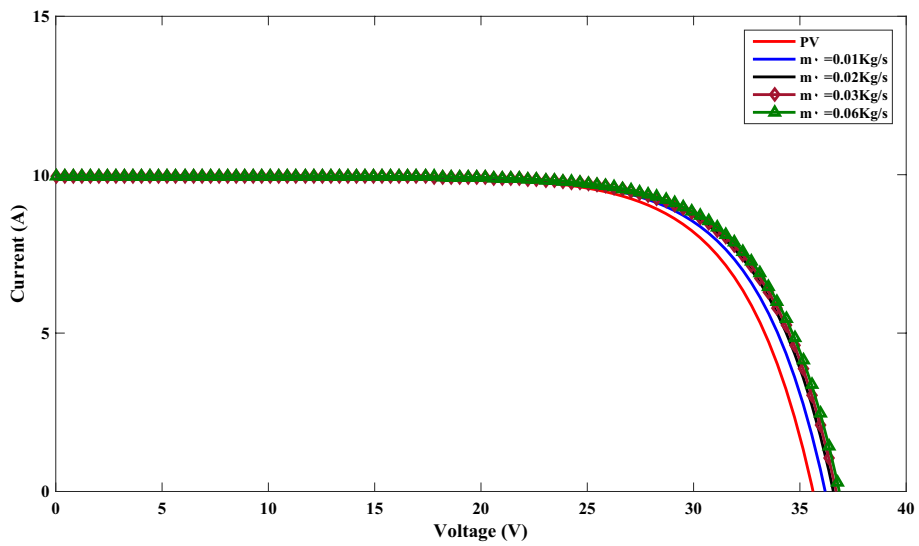


Fig. 7 PV/T collector I - V curves with mass flow rate (Kg/s) variation at STC

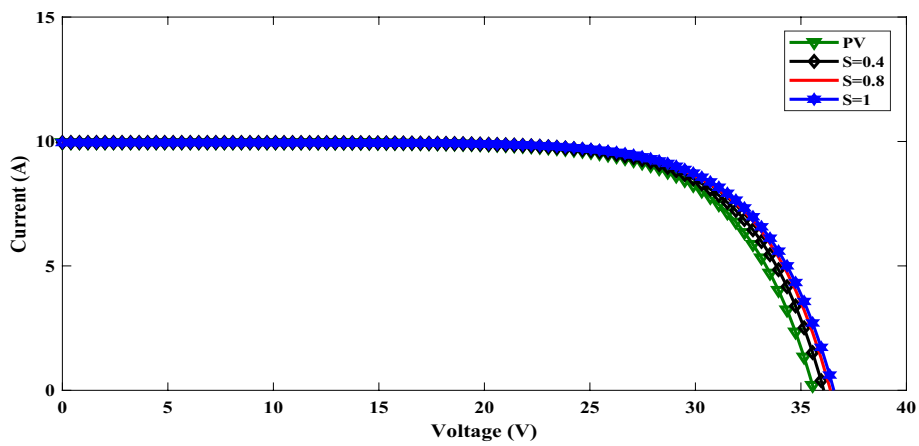


Fig. 8 PV/T collector I - V curves with packing factor variation at STC

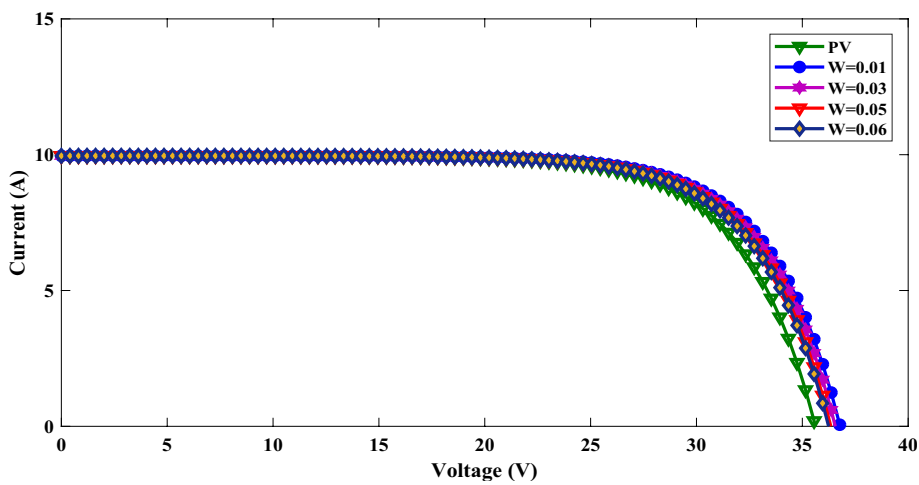


Fig. 9 PV/T collector I - V curves with tube spacing (m) variation at STC

Table 7 Comparing PV/T efficiency with the previous works

Algorithm	η_{elec} (%)	η_{th} (%)	η_T (%)
Proposed work	14.28%	52.8%	89.65%
Fuentes et al. [44]	16.1–19.1%	50–70.4%	66.1–89.5%
Fudholi et al. [45]	11.9–12.4%	41.1–48%	53.6–66.8%
Fudholi et al. [45]	12.2–12.7%	46.4–54.6%	58.4–66.8%
Zhang et al. [46]	9.5	50	59.5
Chow et al. [47]	11	51	62
Aggour et al. [22]	13.43%	35.61%	70.9%

in complexity time, so the new algorithm achieved high and more accurate efficiency within low simulation time as shown in Table 7.

Conclusions

The design parameters for PV/T collectors that aim to produce the maximized thermal and electrical efficiency were presented in this study. The PV/T collector performance is built on numerous design factors that include the fluid flow rate (m), tube diameter (D), spacing between tubes (W), absorber material (K_{abs}), and packing factor (S). With the aim of determining the ideal values for the design parameters, the PV/T collector performance was computed using meta-heuristic optimization techniques, including GA, PSO, GWO, ALO, MVO, DA, MFO, SCA, and WOA. The PV/T collector parameters were optimized with each optimization algorithm, and the obtained parameters were compared with each other, tested, and validated using MATLAB software. The results showed that the most effective optimization algorithms were GWO, ALO, and MFO because they produced the highest thermal and electrical efficiencies. The values of the parameters optimized with the GWO algorithm were the most effective and highest efficiencies; thus, they were considered the most suitable design parameters for PV/T collectors, the results that compared the efficiencies for each algorithm were introduced and discussed. A study of mass flow rate, packing factor, and tube diameter effect with the variation of radiation on the thermal and electrical efficiencies was discussed. Another point also was introduced in this paper that from the electrical behavior as the comparison between stand-alone PV temperature and hybrid PV/T collector temperature, there is a good enhancement in IV curves of the hybrid PV/T collector over the IV curve of stand-alone PV module. In future, we will study the ability to use machine learning and artificial intelligence in PV/T system control and design.

Abbreviations

- PV Photovoltaic module
- GA Genetic algorithm
- GWO Grey wolf algorithm
- MVO Multiverse algorithm
- MFO Moth-flame algorithm
- WOA Whale algorithm
- PV/T Photovoltaic/thermal collector
- PSO Particle swarm algorithm
- ALO Ant-lion algorithm
- DA Dragonfly algorithm
- SCA Sine-cosine algorithm

Acknowledgements

Not applicable.

Author contributions

Heba S Aggour contributed to methodology, software, validation, formal analysis, investigation, data curation, writing—original draft, writing—review and editing, and visualization. Doaa M Atia performed review and editing, and visualization. Hanaa M. Farghally performed investigation, review and editing. M. Soliman contributed to conceptualization and investigation. Mahmoud M. Omar contributed to conceptualization, investigation, and review.

Funding

Not applicable.

Availability of data and materials

All data generated are included in the paper.

Declarations**Competing interests**

The authors declare that they have no known competing financial interests or personal relationships that could have appeared to influence the work reported in this paper.

Received: 3 May 2024 Accepted: 4 June 2024

Published online: 12 June 2024

References

- Wolf M (1976) Performance analyses of combined heating and photovoltaic power systems for residences. *Energy Convers* 16(1–2):79–90. [https://doi.org/10.1016/0013-7480\(76\)90018-8](https://doi.org/10.1016/0013-7480(76)90018-8)
- Solanki S, Dubey S, Tiwari A (2009) Indoor simulation and testing of photovoltaic thermal (PV/T) air collectors. *Appl Energy* 86(11):2421–2428. <https://doi.org/10.1016/j.apenergy.2009.03.013>
- Tiwari GN, Al-Helal IM (2015) Analytical expression of temperature dependent electrical efficiency of N-PVT water collectors connected in series. *Sol Energy* 114:61–76. <https://doi.org/10.1016/j.solener.2015.01.026>
- Fudholi A, Sopian K, Yazdi H, Ruslan M, Ibrahim A, Kazem A (2014) Performance analysis of photovoltaic thermal (PVT) water collectors. *Energy Convers Manag* 78:641–651. <https://doi.org/10.1016/j.enconman.2013.11.017>
- Al-Waeli A, Kazem A, Chaichan T, Sopian K (2019) Experimental investigation of using nano-PCM/nanofluid on a photovoltaic thermal system (PVT): technical and economic study. *Therm Sci Eng Progress* 11:213–230. <https://doi.org/10.1016/j.tsep.2019.04.002>
- Maadi S, Kolahan A, Passandideh-Fard M, Sardarabadi M, Moloudi R (2017) Characterization of PVT systems equipped with nanofluids-based collector from entropy generation. *Energy Convers Manag* 150:515–531. <https://doi.org/10.1016/j.enconman.2017.08.039>
- Jouhara H, Milko J, Danielewicz J, Sayegh M, Szulgowska-Zgrzywa M, Ramos J, Lester S (2016) The performance of a novel flat heat pipe based thermal and PV/T (photovoltaic and thermal systems) solar collector that can be used as an energy-active building envelope material. *Energy* 108:148–154. <https://doi.org/10.1016/j.energy.2015.07.063>
- Liu W, Yao J, Jia T, Zhao Y, Dai Y, Zhu J, Novakovic V (2023) The performance optimization of DX-PVT heat pump system for residential heating. *Renew Energy* 206:1106–1119. <https://doi.org/10.1016/j.renene.2023.02.089>
- Chinipardaz M, Amraee S (2022) Study on IoT networks with the combined use of wireless power transmission and solar energy harvesting. *Sādhanā* 47:1–16. <https://doi.org/10.1007/s12046-022-01829-y>
- Shahsavari A, Talebizadeh P, Tabaei H (2013) Optimization with genetic algorithm of a PV/T air collector with natural air flow and a case study. *J Renew Sustain Energy* 5:023118. <https://doi.org/10.1063/1.4798312>
- Cao Y, Kamrani E, Mirzaei S, Khandakar A, Vaferi B (2022) Electrical efficiency of the photovoltaic/thermal collectors cooled by nanofluids: machine learning simulation and optimization by evolutionary algorithm. *Energy Rep* 8:24–36. <https://doi.org/10.1016/j.egy.2021.11.252>
- Karathanassis K, Papanicolaou E, Belessiotis V, Bergeles C (2013) Multi-objective design optimization of a micro heat sink for concentrating photovoltaic/thermal (CPVT) systems using a genetic algorithm. *Appl Therm Eng* 59(1–2):733–744. <https://doi.org/10.1016/j.applthermaleng.2012.06.034>
- Khaki M, Shahsavari A, Khanmohammadi S, Salmanzadeh M (2017) Energy and exergy analysis and multi-objective optimization of an air based building integrated photovoltaic/thermal (BIPV/T) system. *Sol Energy* 158:380–395. <https://doi.org/10.1016/j.solener.2017.09.056>
- Vera J, Laukkanen T, Sirén K (2014) Multi-objective optimization of hybrid photovoltaic–thermal collectors integrated in a DHW heating system. *Energy Build* 74:78–90. <https://doi.org/10.1016/j.enbuild.2014.01.011>
- Singh S, Agarwal S, Tiwari G, Chauhan D (2015) Application of genetic algorithm with multi-objective function to improve the efficiency of glazed photovoltaic thermal system for New Delhi (India) climatic condition. *Sol Energy* 117:153–166. <https://doi.org/10.1016/j.solener.2015.04.025>
- Sohani A, Dehnavi A, Sayyaadi H, Hoseinzadeh S, Goodarzi E, Garcia D, Groppi D (2022) The real-time dynamic multi-objective optimization of a building integrated photovoltaic thermal (BIPV/T) system enhanced by phase change materials. *J Energy Stor* 46:103777. <https://doi.org/10.1016/j.est.2021.103777>
- Sarhaddi F, Farahat S, Ajam H, Behzadmehr A, MahdaviAdeli M (2010) An improved thermal and electrical model for a solar photovoltaic thermal (PV/T) air collector. *Appl Energy* 87(7):2328–2339. <https://doi.org/10.1016/j.apenergy.2010.01.001>

18. Sattar M, Rehman A, Ahmad N, Mohammad A, AlAhmadi A, Ullah N (2022) Performance analysis and optimization of a cooling system for hybrid solar panels based on climatic conditions of Islamabad, Pakistan. *Energies* 15:6278. <https://doi.org/10.3390/en15176278>
19. Assareh E, Jafarian M, Nedaei M, Firoozzadeh M, Lee M (2022) Performance evaluation and optimization of a photovoltaic/thermal (PV/T) System according to climatic conditions. *Energies* 15:7489. <https://doi.org/10.3390/en15207489>
20. Yazdanifard F, Ebrahimnia-Bajestan E, Ameri M (2016) Investigating the performance of a water-based photovoltaic/thermal (PV/T) collector in laminar and turbulent flow regime. *Renew Energy* 99:295–306. <https://doi.org/10.1016/j.renene.2016.07.004>
21. Farghally HM, Ahmed NM, El-Madany HT, Atia DM, Fahmy FH (2016) Design and sensitivity analysis of photovoltaic/thermal solar collector. *Int Energy J* 15(1):21–32
22. Aggour H, Atia D, Farghally H, Omar M, Elbendary F (2022) Optimal design and feasibility analysis of PV/T based tree seed algorithm. *Int J Ambient Energy* 43(1):6709–6723
23. Veeken L (2014) Technical and economic evaluation of different utilization options based on combined photovoltaic and solar thermal (PV/T) systems for the residential sector. *Energy Science MSc*
24. New and renewable energy authority, ministry of electricity and energy, Egyptian solar radiation atlas, Cairo, Egypt (1998)
25. Gulbas O, Hames Y, Furat M (2020) Comparison of PI and super-twisting controller optimized with SCA and PSO for speed control of BLDC motor. In: 2nd international congress on human-computer interaction, Optimization and robotic applications, proceedings
26. Sen M, Kalyoncu M (2019) Grey wolf optimizer based tuning of a hybrid LQR-PID controller for foot trajectory control of a quadruped robot. *Gazi Univ J Sci* 32(2):674–684
27. Bergamini M, Bonfim M, Leandro G, de Oliveira J (2018) Identification of nonlinear system using evolutionary differential and grey cobem-2017–2029 identification of nonlinear system using evolutionary
28. Li L, Sun L, Guo J, Qi J, Xu B, Li S (2017) Modified discrete grey wolf optimizer algorithm for multilevel image thresholding. *Comput Intell Neurosci* 2017(1):3295769
29. Mirjalili S, Mirjalili S, Lewis A (2014) Grey wolf optimizer. *Adv Eng Softw* 69:46–61
30. Reddy D, Reddy V, Manohar G (2018) Ant Lion optimization algorithm for optimal sizing of renewable energy resources for loss reduction in distribution systems. *J Electr Syst Inf Technol* 5(3):663–680
31. Kavuturu K, Narasimham P (2020) Multi-objective economic operation of modern power system considering weather variability using adaptive cuckoo search algorithm. *J Electr Syst Inf Technol* 7:11. <https://doi.org/10.1186/s43067-020-00019-2>
32. Ullah I, Hussain I, Uthansakul P, Riaz M, Khan M (2020) Exploiting multi-verse optimization and sine-cosine algorithms for energy management in smart cities. *Appl Sci* 10(6):2095
33. Mirjalili S, Mohamad S, Hatamlou A (2016) Multi-verse optimizer: a nature-inspired algorithm for global optimization. *Neural Comput Appl* 27:495–513. <https://doi.org/10.1007/s00521-015-1870-7>
34. Cigdem A, Gulcan H (2019) A modified dragonfly optimization algorithm for single- and multiobjective problems using Brownian motion. *Comput Intell Neurosci* 2019:1–7
35. Debnath S, Baishya S, Sen D, Arif W (2020) A hybrid memory based dragonfly algorithm with differential evolution for engineering application. *Eng Comput* 37(4):2775–2802
36. Khunkitti S, Watson R, Chatthaworn R, Premrudeepreechacharn S, Siritarativat A (2019) An improved DA-PSO Optimization approach for unit commitment problem. *Energies* 12(12):2335. <https://doi.org/10.3390/en12122335>
37. Shehab M, Abualigah L, Al H, Hamzeh H, Mohammad A (2020) Moth-flame optimization algorithm: variants and applications. *Neural Comput Appl* 32(14):9859–9884
38. Hassanin A, Gaber T, Mokhtar U (2017) An improved moth flame optimization algorithm based on rough sets for tomato diseases detection. *Comput Electron Agric* 136:86–96
39. Aydin O, Gozde H, Dursun M, Cengiz M (2019) Comparative parameter estimation of single diode pv-cell model by using sine- cosine algorithm and whale optimization algorithm. pp 6–9. <https://doi.org/10.1109/ICEEE2019.2019.00020>
40. Mohammed H, Rashid T (2020) A novel hybrid GWO with WOA for global numerical optimization and solving pressure vessel design. *Neural Comput Appl* 32(18):14701–14718. <https://doi.org/10.1007/s00521-020-04823-9>
41. Mosaad A, Attia M, Abdelaziz A (2019) Whale optimization algorithm to tune PID and PID a controllers on AVR system. *Ain Shams Eng J* 10(4):755–767. <https://doi.org/10.1016/j.jasej.2019.07.004>
42. Soleimanian F, Gholizadeh H (2019) A comprehensive survey: whale optimization algorithm and its applications. *Swarm Evol Comput* 48:1–24. <https://doi.org/10.1016/j.swevo.2019.03.004>
43. Butti D, Mangipudi S, Rayapudi S et al (2023) An improved whale optimization algorithm for the model order reduction of large-scale systems. *J Electr Syst Inf Technol* 10:29. <https://doi.org/10.1186/s43067-023-00097-y>
44. Fuentes M, Vivar M, de la Casa J, Aguilera J (2019) An experimental comparison between commercial hybrid PV-T and simple PV systems intended for BIPV. *Renew Sustain Energy Rev* 93:110–120. <https://doi.org/10.1016/j.rser.2018.05.021>
45. Fudholi A, Sopian K, Yazdi MH, Ruslan MH, Ibrahim A, Kazem H (2014) Performance analysis of photovoltaic thermal (PV/T) water collectors. *Energy Convers Manag* 78:641–651. <https://doi.org/10.1016/j.enconman.2013.11.017>
46. Zhang X, Zhao X, Smith S, Xu J, Yu X (2012) Review of R&D progress and practical application of the solar photovoltaic/thermal (PV/T) technologies. *Renew Sustain Energy Rev* 16(1):599–617. <https://doi.org/10.1016/j.rser.2011.08.026>
47. Chow T, Ji J, He W (2007) Photovoltaic–thermal collector system for domestic application. *J Sol Energy Eng* 129:205–209. <https://doi.org/10.1115/1.2711474>

Publisher's Note

Springer Nature remains neutral with regard to jurisdictional claims in published maps and institutional affiliations.